BIMA memo 92; ATA memo 52. - 30oct02

Allen Telescope Array Imaging

Melvyn Wright

Radio Astronomy laboratory, University of California, Berkeley, CA, 94720

ABSTRACT

In this memo, we review the imaging requirements, calibration procedures, and processing options for the Allen Telescope Array. The array has excellent *uv* coverage and a very high data rate which will rapidly saturate conventional human data reduction and imaging. The array should produce final, calibrated images as its normal output. Imaging with the ATA was simulated for a range of sources. The performance of MIRIAD running on modern PC's appears adequate for the ATA, but not by a large factor. Efficient software is required.

1. Introduction

The Allen Telescope Array (ATA) is being designed as an array of 350 6-m antennas with antenna spacings from $\sim$ 10 to 900 m. Wide bandwidth receivers and antenna feeds deliver an instantaneous bandwidth from 0.5 to 11.2 GHz to beamformers, correlators and spectrum analyzers.

Multiple backends allow simultaneous imaging observations, pulsar observations, point source spectroscopy, and SETI searches. The wide field-of-view, the ability to observe anywhere in the instantaneous bandwidth of the feed, and the large blocks of observing time that will be available on the ATA are ideally suited to making large surveys and to monitoring temporal variations in a wide variety of sources. The array configuration has been designed to give a Gaussian beam with very low sidelobes and excellent imaging performance. A more detailed discussion of the scientific and technical motivations for the design of the telescope is given elsewhere.

In the following sections we discuss the requirements, calibration procedures, and processing options for astronomical imaging from a radio astronomy perspective. Other, more innovative methods may evolve for large N arrays, but at least this approach provides a basis for evaluating the requirements and performance for imaging with the ATA. We seek architectures and software solutions which are scalable to even larger arrays such as the SKA.

2. Correlator

Astronomical imaging will be implemented using a digital correlator. For a sparse array, with filling factor $350 \times (6m/900m)^2$ and irregular antenna spacing, sampling the correlation function, gridding the averaged *uv* data, and using FFT algorithms is more efficient than direct imaging. The full RF bandwidth (11 GHz) in both polarizations is transmitted to the processing center via wide-band analog optical fiber, where it is digitized into 4 dual-polarization, 105 MHz wide, bands with 8-bit sampling. The correlator is an FX design with up to 1024 frequency channels in bandwidths up to 100 MHz. We require excellent isolation of frequency channels for RFI excision. The correlator uses a polyphase filterbank providing better than 60 db isolation between the frequency channels, which are digitized into 4 bits. The spectra from the polyphase filter are routed through a switch into 350 cross correlators. Each cross correlator processes up to 3 frequency channels for all 350 x 351 / 2 correlations including the autocorrelations for each antenna. The correlation functions are accumulated into 32-bit words for further processing.

3. Data Sampling

In order to observe transient events, search for slow pulsars, and for interference mitigation, the correlator should be capable of fast dump times $\sim$ 10 ms. The normal dump times for most astronomical observations will range from 1 to 1024s. In this mode we should be able to read out 32-bit real, 32-bit imaginary data for all baselines, with all four Stokes parameters. The size of a *uv* sample $(baselines \times channels \times polarizations) = 350^2/2 \times 1024 \times 4 \times 2$ complex words, = 2 Gbytes for 32-bit words.

The Nyquist sample interval for the *uv* data is $\delta uv = D/2\lambda$, where D is the antenna diameter. The Nyquist sampling rate $\sim baseline/\lambda/(D/2\lambda) \times sdot$, where $sdot = 2\pi/24/3600$. For a baseline $\sim$ 700 m the Nyquist sample interval is 1 minute. With a 30s sample interval the data rate is 0.5 Gbit/s; for a 10 ms sample, the rate is 1.5 Tbit/s.

These rates can be reduced by using data compression, for example using 16-bit scaled integers reduces the data by a factor 2, or by reducing the number of channels, or polarizations which are read out. For some projects we will want to read out and store the averaged visibility data, but for most applications the data are processed into images.

4. Images

The array has excellent *uv* coverage and a very high data rate which will rapidly saturate any conventional human data reduction and imaging. The array should produce final, calibrated images as its normal output.

The size of a single field, FWHM image $\sim$ 256 x 256. For mosaicing we want to make images down to 5% or even 1% of the primary beam pattern to obtain good image fidelity. The image size is then $\sim$ 700 – 1500 with 3 pixel per beam sampling. For FWHM images with 1024 spectral channels and 4 polarizations the image size is 1 Gbyte for 32-bit words. Note that this implies that the 4 polarizations have been reduced to real valued Stokes parameters, otherwise the crossed linear polarizations, yield complex images of $I, Q, U, \pm jV$, and polarization leakage terms.

The FWHM image data is about the same size as the *uv* data, so that images instead of *uv* data could be read out and stored at the Nyquist rate without increasing the data volume. In many cases, images can be integrated over time or frequency channels, greatly reducing the data rate. Although some observations may require the *uv* data and not images, the data rate must eventually be reduced in order for the astronomer to assimilate and analyze the observations. In searching for time variable sources, we want to make images of the variance in each pixel from rapidly sampled data. Variance images could also be made as a standard data product for other observations, and serve as interference and serendipitous variability searches.

5. Calibration

The high data rate and the need to apply gain (amplitude and phase), bandpass, polarization leakage, and Stokes conversions in order to average the data over antennas (for the beam formers), time, frequency channels, or polarizations, strongly suggests that the calibrations be applied as the data are acquired in close to real time. Averaging over time or frequency may be required to obtain a sufficient signal to noise ratio to derive the calibrations. The measured correlation, $V' = G(time, frequency, polarization...) \times V$, where V is the true visibility and G is the calibration factor. If the correlator closure errors are small, the calibration factor can be expressed as antenna based calibrations, $G = g_i \times g_j$ for each antenna pair (i, j). Usually, the frequency (passband), and polarization calibrations are slow functions of time, and we can separate the calibrations into antenna dependent gains $g(time)$, passband and polarization calibrations. System components can be measured in the laboratory, but the final calibrations of the whole system are made using astronomical sources.

5.1. Calibration of Antenna Gains

In this section we discuss the calibration of the antenna gains, the amplitude and phase variations, $g(time)$ associated with each antenna. Although the telescope structure and electronics are expected to be stable, optical fiber components on the antennas may require more frequent calibration. Atmospheric phase fluctuations from water vapor at high frequencies and the ionosphere at low frequencies occur on time scales as short as $\sim$ 1 second. The tropospheric water vapor fluctuations are well measured at Hat Creek using the millimeter array. The RMS path length over

a 5 min interval on a 1 km baselines $\sim$ 1 mm in good, winter observing condition (12 degrees of phase at 10 GHz). There are large seasonal and weather related variations, with phase fluctuations an order of magnitude larger on summer afternoons. The ionospheric pathlength variations scale as λ^2, and are larger than those due to water vapor at frequencies below about 1 GHz. There are large variations in the seeing related to diurnal, seasonal and solar activity.

The antenna gain is measured by observing a source with known position and structure, typically an unresolved quasar. Assuming Tsys=40 K, 100 MHz bandwidth, and 350 antennas, the RMS sensitivity is 0.25 mJy in 1 minute. For antenna based calibration, the sensitivity is 5 mJy $\mathrm{min}^{-0.5}$ in a 100 MHz bandwidth. Simulations show that an RMS phase error of 6 degrees or an RMS amplitude error of 10% gives a $\sim$ 1% reduction in the synthesised beam (or beam former) amplitude, and less than 1% increase in the RMS sidelobe level. A 6 degree phase error is equivalent to a surface error $\lambda/60$. This is an acceptable level of degradation for the beam formers; larger losses in forward gain will result from interference mitigation. A calibration error of 6 degrees or 10 % in amplitude requires a SNR $\sim$ 10 which can be obtained with a 1 minute integration on a 50 mJy source, or a 6 second integration on a 5 Jy source. The calibration might be made at a different frequency from the target source observations. In this case a calibration of the relative gain between the calibration and target frequencies is also required. The calibration solutions need to be passed to the control system on timescales of seconds.

5.2. Self Calibration of Antenna Gains

We can often use self calibration on the target source to determine the antenna gains, $g(time)$, from the measured correlations and a model of the source brightness distribution. In many cases continuum sources in the same field of view as the target source can be used to calibrate the antenna gains. Kellerman gives $N(S) = 60S^{1.5}sr^{-1}$; implying, on average, about 8 sources brighter than 50 mJy within the 136 arcmin primary beam at 1.4 GHz.

We simulated ATA observations to test self calibration using a 136 arcmin field containing 266 sources from the NVSS sky survey as a source model. We generated uv data with added thermal noise appropriate for the ATA with 100 MHz bandwidth in a 1 minute integration, and 30 degree RMS of phase noise. The data were self calibrated, imaged and compared with the source model convolved to the same resolution. With 3 iterations of self calibration, the residual phase error was less than 1 degree and the difference between the calibrated image and the source model was consistent with the thermal noise. To test the performance of the algorithm we reduced the thermal noise by a factor 10. The image and the model were consistent with the theoretical noise 1.6 10^{-5} Jy. We also simulated data with increased noise corresponding to 10 MHz and 1 MHz bandwidths. Self calibration fails when the errors in the derived gains are greater than the thermal noise in the data. The data simulation and the 3-iteration self calibration each took $\sim$ 1 minute on a Linux based PC using standard MIRIAD software, so that this calibration could keep up with 1-minute observations.

Although self calibration works well for this simple source model, it will fail if the source model is too complex. Large scale structure can be filtered out by using only long baselines, but for the ATA, this greatly reduces the number of baselines and the efficacy of self calibration. For the ATA the median baseline ~ 270 m. Sidelobes from a nearby strong source can also cause problems for self calibration. The success of self calibration will depend on the individual situation, source structure, and scientific goals. The ATA is quite different from the VLA where strong compact continuum sources can often be used for self calibration. For spectral line observations the signal may be distributed in different structures over a range of frequency, e.g. HI observations in a rotating galaxy. Multiple frequency channels can simultaneously be used to determine the antenna gains using an image cube. The MIRIAD self calibration algorithm supports a source model comprised of multiple image cubes, as are obtained from mosaiced spectral line observations. For an unknown source distribution, self calibration will be improved by using the best estimate of the source structure formed using all the relevant *uv* data. In this case we need to store the *uv* data. It is still of considerable interest to make images as the data are collected, but the calibration can be improved after the observations are complete.

5.3. Polarization Calibration

The relatively high polarization leakage for the 11 GHz wideband feeds requires that full polarization data be sampled and corrected for leakage in order to obtain the best image fidelity even if only total intensity, Stokes I, is required. In simple cases it may suffice to observe a single linear polarization. In general, polarization calibrations require observations over a range of parallactic angles in order to separate source and instrumental polarization. If the polarization leakage is stable, then a full polarization calibration need only be made at infrequent intervals. The polarization calibration is a function of observing frequency and can be applied from lookup tables and applied to the *uv* data before it is written out or imaged.

5.4. Passband Calibration

The instrumental frequency response across the 100 MHz bandwidth includes contributions from receiver and backend components. Both RF and IF components are expected to have stable passbands which can be measured in the laboratory. The frequency response of the whole system can be calibrated from observations of a strong achromatic astronomical source at intervals determined from the stability of the bandpass and the requirements of the astronomical observations. The passband will be a function of the observing frequency and can also be applied to the *uv* data before it is saved or imaged.

6. Calibration and Imaging Architecture

We are investigating various system architectures for processing the *uv* data. After cross correlation, the *uv* data are time-averaged for each spectral channel. Calibration and wideband imaging requires averaging over frequency channels, but for spectral line observations images can be made for individual (or averages over a few) frequency channels. These requirements suggest alternate architectures: wide-band calibration and imaging requires the *uv* data from all frequency channels, and suggests a high data rate into a central processor, whilst spectral line imaging can be made for each frequency with distributed processors and a more modest data rate. The processors might be installed as (i) mezzanine cards on each correlator board, (ii) a cpu in each compact PCI crate, (iii) a cpu connected to each correlator board via ethernet, or (iv) a central processing cluster.

The distributed architectures (i - iii), are an obvious choice for spectral line processing; images can be made independently, averaged in time and read out at a modest data rate. Wideband images can be made by averaging spectral images; MFS images may be required in any case for large fields of view. For antenna based calibrations, complex gains could be derived for averages of groups of frequency channels, thus reducing the calibration data by a factor 350 with the same time resolution. The complex gains can be averaged in time and frequency to obtain sufficient SNR to be applied to incoming data.

Option (iv) requires the full *uv* data rate, and a potential bottleneck into the central processing cluster, although this is the most versatile and easy to upgrade. The relative investment of time and money for correlator ($\sim \$10^6$) and postprocessing ($\sim \$10^5$), suggests that the postprocessing hardware might be upgraded several times during the lifetime of the correlator hardware. We require that the postprocessing hardware be easily upgraded and that the software be easily transferred to new postprocessing hardware.

We require that it be possible to install existing software, which is well tested and efficient. We also require that it be easy to install new processing algorithms since the most innovative experiments will inevitably need new or modified software. Easily modified software and access to astronomers is a key to using the ATA for novel experiments.

7. Archiving

With 30s sampling the full data rate $\sim$ 1 Gbyte/s for FWHM images or 2 Gbyte/s for *uv* data. i.e. 120 to 240 Gbytes/hour. The archiving (and data retrieval) requirements can be greatly reduced by integrated over time or frequency channels before the data are stored. The integration time may vary from as rapid as possible, to several days per image. For the current science proposals, the average integration time $\sim$ 1 hour per image requiring $\sim$ 24 Gbytes/day. The science proposals include several whole sky, or galactic plane surveys. At λ 21 cm, the primary beamwidth $\sim$ 2.5

degrees, so each survey will comprise $\sim 10^4$ 1-Gbyte images which need long term storage for data analysis.

8. Imaging simulation

Imaging with the ATA was simulated for a range of source sizes and declinations using the MIRIAD software. Figure 1 shows a Mosaic MFS Image of Cas A scaled up 40 x real size, imaged with the ATA. We generated *uv* data for a snaphot observation by the ATA using a VLA image of Cas A as source model.

We used a mosaic observation in a hexagonal pointing pattern with 0.96 degree spacings at an observing frequency 1.42 GHz. A 1 min integration at each of 7 pointing positions generated 1221500 *uv* data samples with 20 frequency channels. Thermal noise appropriate for the ATA was added to the *uv* data. The *uv* data was Fourier transformed to make images and deconvolved using Maximum Entropy (MEM) algorithms. The original image model was convolved to the same resolution by a Gaussian restoring beam and subtracted from the deconvolved image. The residual imaging errors are characterized by the total recovered flux, peak flux density and the RMS residuals. The results are pipelined into tables. The mosaicing process, the simulated images and the residual images are displayed on the terminal, and the images are saved on disk for further analysis.

The simulations were made on a PC running MIRIAD scripts under the LINUX operating system. For single field images the requirements are modest. Simulating the *uv* data for 100 spectral channels with 1 minute integration takes $\sim$ 35s. Fourier transform to a 256 x 256 x 100 channel image takes $\sim$ 30s, and deconvolution using the CLEAN algorithm takes $\sim$ 60s for 100 spectral channels. For mosaic images the requirements are more demanding. Generating the *uv* data for a 7-pointing mosaic takes $\sim$ 60s. Fourier transform to a 1585 x 1510 mosaic image and 2049 x 2049 x 7 pointing beam takes only $\sim$ 47s, but the Maximum Entropy (MEM) deconvolution with 200 iterations takes over 1 hour to converge. Fortunately, because of the low sidelobe level for the ATA synthesised beam, such deconvolution will only be needed for bright sources. Most images of low brightness emission will be limited by thermal noise and will not require deconvolution. The performance of MIRIAD running on modern PC's appears adequate for the ATA, but not by a large factor. Efficient software is required.

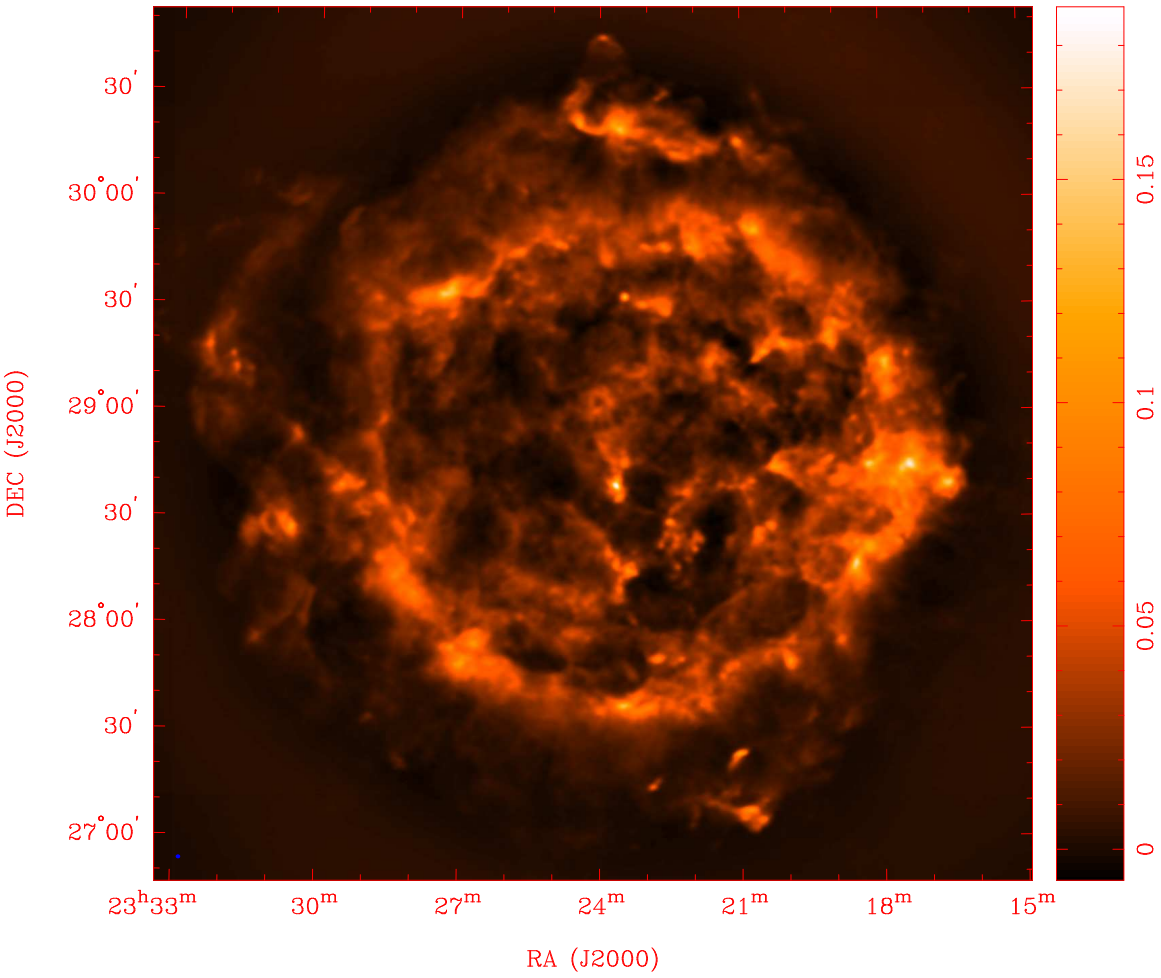

Fig. 1.— A mosaic MFS Image of CASA scaled up 40 x real size, imaged with the ATA at 1.42 GHz. The image is 4 degrees on a side. The synthesised beam FWHM, 77 x 78 arcsec is shown in the lower left corner.